High-Accuracy Measurement of Atomic Polarizability in an Optical Lattice Clock

J. A. Sherman,[1,*] N. D. Lemke,[1,2] N. Hinkley,[1,2] M. Pizzocaro,[3] R. W. Fox,[1] A. D. Ludlow,[1] and C. W. Oates[1]

[1]*National Institute of Standards and Technology, 325 Broadway, Boulder, Colorado 80305, USA*
[2]*University of Colorado, Department of Physics, Boulder, Colorado 80309, USA*
[3]*Politecnico di Torino, Corso duca degli Abruzzi 24, 10125 Torino, Italy*
(Received 12 December 2011; published 13 April 2012)

Presently, the Stark effect contributes the largest source of uncertainty in a ytterbium optical atomic clock through blackbody radiation. By employing an ultracold, trapped atomic ensemble and high stability optical clock, we characterize the quadratic Stark effect with unprecedented precision. We report the ytterbium optical clock's sensitivity to electric fields (such as blackbody radiation) as the differential static polarizability of the ground and excited clock levels $\alpha_{\text{clock}} = 36.2612(7)$ kHz (kV/cm)$^{-2}$. The clock's uncertainty due to room temperature blackbody radiation is reduced by an order of magnitude to 3×10^{-17}.

An atom immersed in an electric field $\vec{E}_a$ becomes *polarized*—the electronic wave function is stretched into alignment with the field. Generally, energies of the lowest-lying electronic quantum states $|i\rangle$ are reduced by $-\frac{1}{2}\alpha_i^{(0)}E_a^2$ (see Fig. 1) where $\alpha_i^{(0)}$ is termed a state's static polarizability [1]. The scaling of the Stark effect is quadratic because $\vec{E}_a$ is responsible for inducing, and also interacting with, an atomic dipole moment.

Neutral atom lattice clocks [2] employ 10^3–10^5 ultracold alkaline-earth atoms tightly confined in an optical standing wave potential so their intrinsically narrow, largely imperturbable, $^1S_0 \leftrightarrow {}^3P_0$ transitions [3] may establish stable and accurate frequency and time references [4,5]. In analogy to a pendulum's oscillation slowing due to thermal expansion, a ytterbium lattice clock slows when electrically stretched, or polarized, by thermal blackbody radiation (BBR) fields [6,7]. This phenomenon has been measured in cesium fountain primary standards [8,9] and other optical transitions [1,10,11].

No shield at finite temperature protects a clock atom from the time varying electric field of BBR, the electromagnetic energy absorbed and reemitted by all matter in thermal equilibrium according to the Stefan-Boltzmann law [12]. Inside a hollow shell of opaque matter (a *blackbody*), the time-averaged electric field intensity depends strongly on the absolute temperature T [13], $\langle E^2 \rangle_T \approx$ $(8.319$ V/cm$)^2(T/300$ K$)^4$. Near room temperature, the spectrum of radiation is peaked strongly near 9.6 μm, far detuned from strong electronic transitions in ytterbium.

The ytterbium clock frequency ($\nu \approx 518$ THz) is shifted by the net BBR Stark effect of the two clock states, which can be expressed as

$$\Delta\nu_{\text{BBR}} = -\frac{1}{2}(\alpha_e^{(0)} - \alpha_g^{(0)})\langle E^2 \rangle_T [1 + \eta_{\text{clock}}(T)], \quad (1)$$

where $\alpha_{g,e}^{(0)}$ are the static polarizabilities of ground and excited states ($^1S_0$ and $^3P_0$, respectively), and $\eta_{\text{clock}}(T)$

[7] is a small computed parameter accounting for the dynamic aspect of the BBR field [14]. At room temperature, η_{clock} is at most a 2% contribution to $\Delta\nu_{\text{BBR}} \approx -1.3$ Hz. More significantly, knowledge of $\alpha_{\text{clock}} \equiv \alpha_e^{(0)} - \alpha_g^{(0)}$ is theoretical, and limited to 10% accuracy due to the complexity of this many-electron atom [7,15,16]. The uncertainty in α_{clock} contributed the dominant fractional
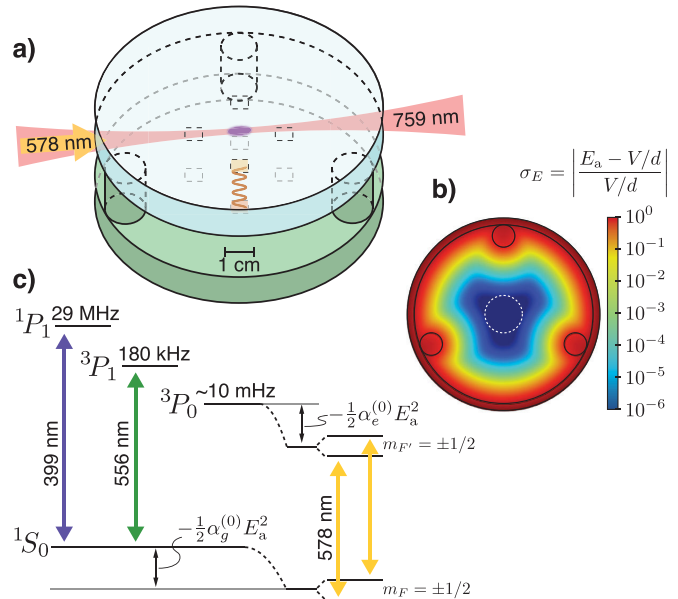

FIG. 1 (color). (a) A scale drawing of transparent conductive electrodes surrounding a one-dimensional optical lattice of ytterbium atoms. Four pairs of metallic pads (one of which is highlighted) allow *in situ* interferometric measurement of the electrode spacing d. (b) Deviations σ_E of the applied electric field E_a from the ideal field created by infinite-planar electrodes become negligible in the central 1 cm region (dashed white circle). (c) Relevant energy levels, laser transition wavelengths, and linewidths ($\Gamma/2\pi$) of ^{171}Yb. Clock states $^1S_0$ and $^3P_0$ are shown Stark shifted by $\vec{E}_a$.

frequency uncertainty, 2.5×10^{-16}, to the optical lattice clock when last evaluated at NIST [6].

To measure α_{clock}, and reduce the clock's uncertainty due to BBR, we fitted electrodes [17] to an existing ytterbium clock apparatus [6]. A voltage V on ideal electrodes spaced by d in vacuum creates an electric field $E_a = V/d$, shifting the clock transition by $\Delta \nu = -\frac{1}{2} \alpha_{\text{clock}} (V/d)^2$. Deviations from this infinite-parallel plane capacitor model are bounded at the 10^{-6} (1 ppm) level by designing a large electrode diameter-to-spacing ratio, ensuring a high degree of parallelism, and centering the atoms radially within the electrodes. Perturbations due to dielectric and conducting mounting structure contribute similar amounts of field uncertainty.

The electrodes, shown in Fig. 1, are composed of rigidly spaced parallel fused silica plates [101.6(1) mm in diameter, better than $\lambda/10$ flatness] featuring a transparent conductive coating on the inner surfaces. The outer surfaces are antireflection coated for all relevant laser wavelengths. The electrode separation, $d = 15.03686(8)$ mm, measured throughout data taking, is maintained by three fused silica rods bonded 45(1) mm from the center axis with hydroxide catalysis [18,19]. d is determined interferometrically by measuring (*in situ*) the free spectral range (fsr) $\nu_{\text{fsr}} = c/2d$ of planar etalons formed by 90% reflective metallic pads (33 nm gold on 2 nm chromium) deposited over the 0.3 nm indium-tin-oxide (ITO) inner electrode faces [17]. Each 6 mm square pad is offset 28 mm from center. An external cavity diode laser is tuned by 17 THz around $\lambda_p = 766$ nm to observe a set of fringes spanning $N_f \approx 1700$ etalon transmission peaks. Each transmission feature, located with a wavelength meter to ± 50 MHz, has a linewidth of 500 MHz, consistent with a finesse $\mathcal{F} \approx 20$. Spacing $\sim$10 observed peaks logarithmically allows an efficient least-squares determination of ν_{fsr}. Systematic wavelength and fringe-center inaccuracy is largely divided down by N_f. Uncertainty in the metal pad thickness contributes 3×10^{-7} uncertainty to d. Gold's index of refraction ($n_r \approx 0.16$) [20] varies gently about λ_p; variations in ν_{fsr} with fringe index due to mirror phase shifts contribute an error of 1.2×10^{-6}. Stray etalons add a similarly sized line-pulling error. Electrode parallelism is constrained by the measured finesse as well as spatially independent pad-pair measurements of d. We resolved no thermal drifts in d.

Thin strips of silver-loaded epoxy join insulated wires to electrode perimeters. Two wires are redundantly bonded to each electrode to establish the sheet resistance of the conductive layer ($R_{\text{ITO}} = 3$ kΩ). The parasitic resistance between the electrodes and the grounded vacuum structure is $R_{\text{leak}} = 316(9)$ GΩ ($R_{\text{leak}} = 14.3(5)$ GΩ) below (above) an observed field-emission threshold occurring near 800 V. Leads to the electrodes have current-limiting resistances of 10 kΩ each; the worst-case E_a error from voltage division is 1.4×10^{-6}. We constructed a regulated

voltage source producing 100 V–1050 V with 1.0×10^{-6} instability over 1 s–1000 s [21].

A clock interrogation cycle (360 ms) begins with slowing, cooling, and trapping ^{171}Yb from an atomic beam with a magneto-optical trap operating first on the $^1S_0 \leftrightarrow {}^1P_1$ transition (399 nm), then on the narrower $^1S_0 \leftrightarrow {}^3P_1$ transition (556 nm). Ultracold atoms (10 μK) are confined by an optical lattice (1D) at the so-called *magic* wavelength near 759 nm resulting in no net ac-Stark shift between $^1S_0$ and $^3P_0$ [3,22]. Atoms are optically pumped into one nuclear-spin state ($m_F = \pm 1/2$) of $^1S_0$. A π-polarized pulse (100 ms) of resonant 578 nm laser radiation coherently excites one of two $\Delta m_F = 0$ transitions (split by 500 Hz by an applied magnetic field $\vec{B}$) to the long-lived $^3P_0$ state (see Fig. 1). A series of laser pulses converts the resulting clock state populations into fluorescence signals which are then normalized against atom number fluctuations [6].

The stabilized 578 nm laser is independently locked to the atomic transition under three interleaved conditions: both electrodes grounded (condition 'A'), and each electrode at high voltage with the other grounded ('B' and 'C'). Each condition, mediated by optocoupled reed relays, lasts $\tau_\nu = 2.9$ s, during which the clock laser maintains a frequency stability approaching 3×10^{-16} [23]. In each period τ_ν, two interrogations are performed on each side of both nuclear-spin spectroscopic features. Slow laser drifts are common to all three integrated error signals, $\Delta \nu_A$, $\Delta \nu_B$, and $\Delta \nu_C$ (see Fig. 2). The quadratic Stark shift is

$$\Delta \nu = \frac{1}{2} (\Delta \nu_B + \Delta \nu_C) - \Delta \nu_A. \qquad (2)$$

The total deviation [24] is used to determine the statistical uncertainty of $\Delta \nu$. For presented data, $\vec{E}_a \parallel \vec{E}_{\text{lattice}}$ (both were perpendicular to $\vec{B}$), though other configurations were examined.

Reversing $\vec{E}_a$ [17] yields information about stray electric fields $\vec{E}_s$ parallel to $\vec{E}_a$ or differential contact potentials [25] (e.g., one electrode may develop a thin layer of ytterbium deposition). The difference $\Delta \nu_B - \Delta \nu_C = 2\alpha_{\text{clock}} \vec{E}_a \cdot \vec{E}_s$ reveals that $|\vec{E}_s \cdot \hat{z}| \approx 0.1$ V/cm (see Fig. 3); temporal drift and weak correlation with $\vec{E}_a$ are observed.

Shifts due to a truly static field $\vec{E}_s$ subtract completely in Eq. (2). However, time dependent changes, notably those correlated with the polarity of $\vec{E}_a$, do not. Because of careful experimental design, we are not aware of any appreciable stray field source with such a correlation. Nevertheless, because an increase in dwell period τ_ν potentially allows an accumulation of unknown stray charge (and thus a correlated stray field), we varied τ_ν over intervals from 0.8 to 12 s and resolved a small but negligible correlation in $\Delta \nu$ at applied fields twice the maximum used for reported data. We observed no systematic variation in the measured
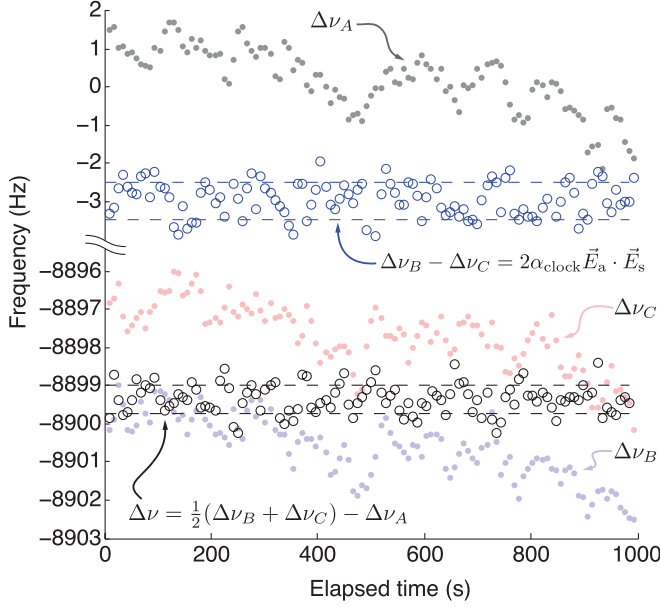
FIG. 2 (color). Integrated clock laser correction signals are shown for $E_a \approx 700.6$ V/cm under three interleaved conditions: both electrodes grounded ('A', grey dots), and each electrode at high voltage with the other grounded ('B' and 'C', blue and red dots). Laser drift, common to these signals, is removed from the quadratic Stark shift signal [black open circles, see Eq. (2)] and the stray field signal $\Delta \nu_B - \Delta \nu_C$ (blue open circles). Dashed lines show standard deviations for these signals. A passive feedforward linear drift canceler reduced clock laser drift to 4 Hz over this 1000 s data run.

polarizability α_{clock} with E_a. We note that for data presented here, E_a remained 3 orders of magnitude below the dielectric strength of fused silica, and 5 orders of magnitude below the characteristic level [26] for ITO electron emission. The time constant for electrode charging is 8 μs. Typically, 100 ms is allowed for settling. Connecting high voltage to both electrodes creates an electric-gradient field; by observing $\Delta \nu < 30$ mHz with 2 kV applied, we constrain the atoms' radial position to ± 10 mm, consistent with visual observations.

Figure 3(a) shows the observed clock frequency shift quadratically as a function of E_a. When fit to a polynomial, the data are consistent with no quartic, cubic, linear, or offset terms—an ideal demonstration of the Stark effect as nondegenerate perturbation theory. No inhomogeneous line broadening is observed with increased shift, so the statistical uncertainty in $\Delta \nu$ reduces as E_a^{-2}. But the uncertainty of the applied voltage (the dominant systematic uncertainty) rises as E_a^2 according to the specifications of our commercial voltmeters. Figure 3(c) plots the polarizability inferred at each E_a. Table I lists the sources of measurement uncertainty at a particular applied field. Taking the mean of all measurements, weighted by the total standard errors, we determine $\alpha_{\text{clock}} = 36.2612(7)$ kHz (kV/cm)$^{-2}$. A least-squares functional fit
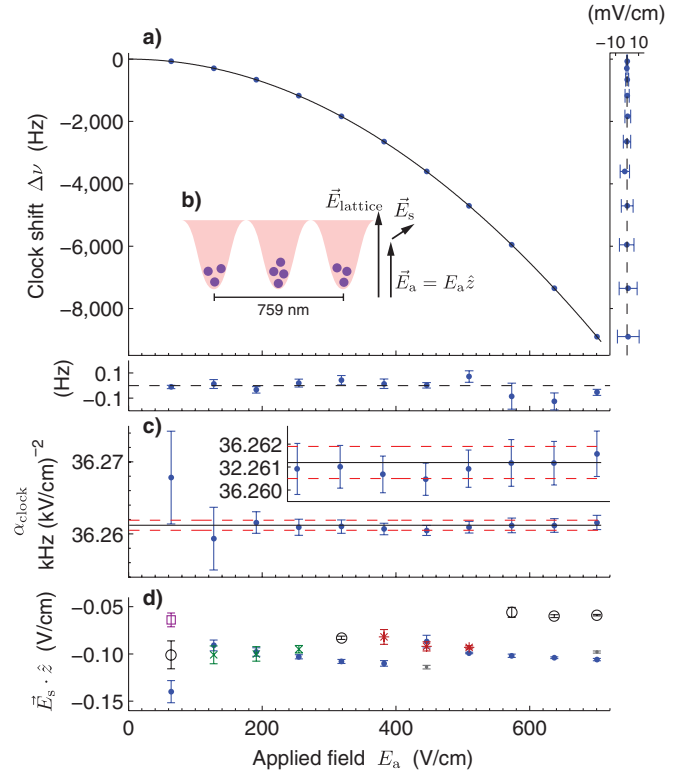

FIG. 3 (color). The clock slows when "stretched." (a) Residuals of a quadratic fit $\Delta \nu = -\frac{1}{2} \alpha_{\text{clock}} E_a^2$ display measurement uncertainties in $\Delta \nu$ (below) and E_a (right). (b) An inset depicts lattice trapped atoms and the relative orientations of $\vec{E}_{\text{lattice}}$, $\vec{E}_a$, and hypothetical static stray field $\vec{E}_s$. (c) At each E_a, we display $\alpha_{\text{clock}} = -2\Delta \nu / E_a^2$ with combined statistic and systematic uncertainties (see Table I). An inset shows data at higher resolution. Solid and dashed lines show the final result and standard error, respectively. (d) The component of a stray field $\vec{E}_s \parallel \vec{E}_a$ is precisely detected upon $\vec{E}_a$ reversal. We observe more temporal variation in E_s than correlation with E_a. Data with different marker styles were acquired on separate days.

[Fig. 3(a)] yields a consistent value for α_{clock}. Table II demonstrates the agreement between this measurement and theoretical predictions.

Neither static nor BBR fields cause spin-magnitude-dependent ($\propto |m_F|^2$) *tensor* Stark shifts because both clock states have insufficient total angular momentum ($F = F' = 1/2$) [27]. Spin-sign-dependent ($\propto m_F$) *vector* Stark shifts are absent as well: BBR has no net polarization and static fields lack the time dependence to be circularly polarized [28]. No opposite-parity states lie close to either clock state so no linear dependence of $\Delta \nu$ on E_a is expected or observed. A third-order effect [29] mixing the polarization due to the optical lattice ($E_{\text{lattice}} \approx 10$ kV/cm) and E_a is expected to cause a 10^{-9} fractional error at the highest E_a, and is further suppressed with linear lattice polarization. A fourth-order term $\Delta \nu \propto E_a^4$ (the *hyperpolarizability*) is responsible for a similarly sized effect. We observed no systematic effect in $\Delta \nu$ upon varying the

TABLE I. Uncertainty budget for a representative datum. Errors in E_a contribute twice the uncertainty as those in $\Delta\nu$ due to the dependence $\alpha_{\text{clock}} = -2\Delta\nu/E_a^2$. This factor of 2 is included in the tabulated quantities below. The total uncertainty in α_{clock}, for the particular measurement shown, is found by summing all contributions in quadrature.

Uncertainty source	$\times 10^{-6}$	Notes or conditions
Shift statistical error	8.3	$\Delta\nu = -3603.77(3)$ Hz (1800 s averaging)
Higher-order Stark shifts	0.01	
Electric field (E_a) errors:		$E_a = 445.836(4)$ V/cm
Voltmeter systematic	16.4	Regulated 670.3966(55) V
R_{leak} voltage division	0.1	$I_{\text{leak}} = 2.1$ nA; 20 kΩ leads
Finite electrode size	1	Atoms centered ± 10 mm
Electrode parallelism	4	$\theta_{\text{wedge}} < 7$ μrad
Electrode deformation	0.8	Warping of fused silica by gravity
Dielectric spacers	2	Perturbation of ideal field due to three fused silica posts
Spacing d (statistical)	1.6	$N_f > 1700$ fringes spanned
Spacing d (systematic)	9	Fringe centering, wave meter accuracy, stray etalons, stability
Etalon probe tilt, ϕ	0.3	$(1 - \cos\phi)$ error, $\phi \ll 0.5$ mrad; retro-coupling single-mode fiber
Yb thermal beam	0.06	Dielectric $(\epsilon_r - 1) \sim 8 \times 10^{-9}$
Stray fields, static	0.04	Uncertainty in $\vec{E}_a$ reversal
Stray fields, varying	2	$\Delta\nu$ correlation with τ_ν
Total uncertainty in α_{clock}	21	

lattice intensity or polarization. We ensured that the atomic density did not systematically vary with application of E_a; such a correlation could introduce contamination from the cold collision shift [30]. We resolved no shift by systematically varying the electrodes between grounded and floating configurations. Finally, we observed no variation in Zeeman splitting with application of E_a.

In practice, precise knowledge of α_{clock} and η_{clock} [see Eq. (1)] is not sufficient to determine the effect of BBR, since knowledge of the thermal environment is limited. Nonuniformities arise due to temperature gradients, a hot effusive oven tip (850 K) and heated viewport (600 K), each about 30 cm away from the trapped atoms, and vacuum walls and viewports with less than unity emissivity and opacity. At $T = 300(1)$ K, $\Delta\nu_{\text{BBR}} = -1.273(17)$ Hz with a dominant effective 1 K uncertainty in T leading to a uncertainty of 3×10^{-17} in the room temperature clock. A cryogenically shielded environment at $T = 77(1)$ K with carefully controlled optical access can reduce the BBR shift uncertainty to the 1×10^{-18} regime [31]. A stray static field of 0.1 V/cm shifts the ytterbium clock transition -0.18 mHz, a fractional change of 4×10^{-19}.

A conductive enclosure at any temperature further ensures these, or smaller, stray static fields [32].

We note that our present uncertainty in α_{clock} is competitive with the best known atomic or molecular polarizability, that of helium [33]. Beyond timekeeping, possible metrological applications of the present work include high voltage measurement without the use of resistive dividers or an atomic electric field meter sensitive at moderate field strengths, in contrast to Rydberg atoms [34] which are most sensitive at very low fields.

TABLE II. Comparison with theoretical predictions. Results are also presented in SI and frequently used *atomic units* (a.u.) [1].

$\alpha_{\text{clock}} \equiv \alpha_e^{(0)} - \alpha_g^{(0)}$ [kHz(kV/cm)$^{-2}$]	(a.u.)	$(10^{-39}$ C m^2/V)	Reference
40.1(3.7)	161(15)	2.65(25)	[15]
38.6(4.0)	155(16)	2.56(26)	[7]
33(13)	134(51)	2.21(84)	[16]
36.2612(7)	145.726(3)	2.402 69(5)	this work

[1] J. Mitroy, M. S. Safronova, and C. W. Clark, J. Phys. B **43**, 202001 (2010).

[2] H. Katori, M. Takamoto, V. G. Palchikov, and V. D. Ovsiannikov, Phys. Rev. Lett. **91**, 173005 (2003).

[3] S. G. Porsev, A. Derevianko, and E. N. Fortson, Phys. Rev. A **69**, 021403 (2004).

[4] T. Udem, R. Holzwarth, and T. W. Hänsch, Nature (London) **416**, 233 (2002).

[5] L. Hollberg, C. W. Oates, G. Wilpers, C. W. Hoyt, Z. W. Barber, S. A. Diddams, W. H. Oskay, and J. C. Bergquist, J. Phys. B **38**, S469 (2005).

[6] N. D. Lemke, A. D. Ludlow, Z. W. Barber, T. M. Fortier, S. A. Diddams, Y. Jiang, S. R. Jefferts, T. P. Heavner, T. E. Parker, and C. W. Oates, Phys. Rev. Lett. **103**, 063001 (2009).

[7] S. G. Porsev and A. Derevianko, Phys. Rev. A **74**, 020502 (2006).

[8] E. Simon, P. Laurent, and A. Clairon, Phys. Rev. A **57**, 436 (1998).

[9] E. J. Angstmann, V. A. Dzuba, and V. V. Flambaum, Phys. Rev. Lett. **97**, 040802 (2006).

[10] T. Rosenband, W. M. Itano, P. O. Schmidt, D. B. Hume, J. C. J. Koelemeij, J. C. Bergquist, and D. J. Wineland, arXiv:physics/0611125.

[11] J. Li and W. A. van Wijngaarden, Phys. Rev. A **53**, 604 (1996).

[12] L. D. Landau and E. M. Lifshitz, *Statistical Physics*, Course in Theoretical Physics Vol. 5 (Butterworth, London, 1980), 3rd ed., Part I.

[13] E. J. Angstmann, V. A. Dzuba, and V. V. Flambaum, Phys. Rev. A **74**, 023405 (2006).

[14] State specific parameters ($\eta_g \approx 0$, $\eta_e = 0.007$) in [7] help to define $\eta_{\mathrm{clock}} \equiv (\eta_e \alpha_e^{(0)} - \eta_g \alpha_g^{(0)})/\alpha_{\mathrm{clock}}$ and compute $\eta_{\mathrm{clock}}(300\ \mathrm{K}) = 0.0145(15)$. We note that η_{clock} most strongly depends on the value of the dipole reduced matrix element $\langle 5d6s\,^3D_1 \| er \| 6s6p\,^3P_0 \rangle$.

[15] V. A. Dzuba and A. Derevianko, J. Phys. B **43**, 074011 (2010).

[16] S. G. Porsev, Y. G. Rakhlina, and M. G. Kozlov, Phys. Rev. A **60**, 2781 (1999).

[17] L. R. Hunter, D. Krause, Jr, K. E. Miller, D. J. Berkeland, and M. G. Boshier, Opt. Commun. **94**, 210 (1992).

[18] D. H. Gwo, U.S. Patent No. 6 284 085 2001.

[19] S. Reid, G. Cagnoli, E. Elliffe, J. Faller, J. Hough, I. Martin, and S. Rowan, Phys. Lett. A **363**, 341 (2007).

[20] L. G. Schulz and F. R. Tangherlini, J. Opt. Soc. Am. **44**, 362 (1954).

[21] P. Horowitz and W. Hill, *The Art of Electronics* (Cambridge University Press, Cambridge, England, 1989) Vol. 2, p. 368.

[22] Z. W. Barber, J. E. Stalnaker, N. D. Lemke, N. Poli, C. W. Oates, T. M. Fortier, S. A. Diddams, L. Hollberg, C. W. Hoyt, and A. V. Taichenachev *et al.*, Phys. Rev. Lett. **100**, 103002 (2008).

[23] Y. Y. Jiang, A. D. Ludlow, N. D. Lemke, R. W. Fox, J. A. Sherman, L. S. Ma, and C. W. Oates, Nature Photon. **5**, 158 (2011).

[24] D. A. Howe, IEEE Trans. Ultrason. Ferroelectr. Freq. Control **47**, 1102 (2000).

[25] L. H. Fisher and R. N. Varney, Am. J. Phys. **44**, 464 (1976).

[26] Y. Y. Lau, Y. Liu, and R. K. Parker, Phys. Plasmas **1**, 2082 (1994).

[27] J. R. P. Angel and P. G. H. Sandars, Proc. R. Soc. A **305**, 125 (1968).

[28] J. E. Stalnaker, D. Budker, S. J. Freedman, J. S. Guzman, S. M. Rochester, and V. V. Yashchuk, Phys. Rev. A **73**, 043416 (2006).

[29] M. V. Romalis and E. N. Fortson, Phys. Rev. A **59**, 4547 (1999).

[30] N. D. Lemke, J. von Stecher, J. A. Sherman, A. M. Rey, C. W. Oates, and A. D. Ludlow, Phys. Rev. Lett. **107**, 103902 (2011).

[31] T. Middelmann, C. Lisdat, S. Falke, J. S. R. Vellore Winfred, F. Riehle, and U. Sterr, IEEE Trans. Instrum. Meas. **60**, 2550 (2011).

[32] J. Lodewyck, M. Zawada, L. Lorini, M. Gurov, and P. Lemonde, IEEE Trans. Ultrason. Ferroelectr. Freq. Control **59**, 411 (2012).

[33] J. W. Schmidt, R. M. Gavioso, E. F. May, and M. R. Moldover, Phys. Rev. Lett. **98**, 254504 (2007).

[34] A. Osterwalder and F. Merkt, Phys. Rev. Lett. **82**, 1831 (1999).